

## Effect of truncating electrostatic interactions on predicting thermodynamic properties of water–methanol systems

Rahbari, A.; Hens, R.; Jamali, S. H.; Ramdin, M.; Dubbeldam, D.; Vlugt, T. J.H.

**DOI**

[10.1080/08927022.2018.1547824](https://doi.org/10.1080/08927022.2018.1547824)

**Publication date**

2019

**Document Version**

Final published version

**Published in**

Molecular Simulation

**Citation (APA)**

Rahbari, A., Hens, R., Jamali, S. H., Ramdin, M., Dubbeldam, D., & Vlugt, T. J. H. (2019). Effect of truncating electrostatic interactions on predicting thermodynamic properties of water–methanol systems. *Molecular Simulation*, 45(4-5), 336-350. <https://doi.org/10.1080/08927022.2018.1547824>

**Important note**

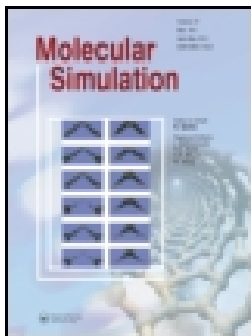
To cite this publication, please use the final published version (if applicable). Please check the document version above.

**Copyright**

Other than for strictly personal use, it is not permitted to download, forward or distribute the text or part of it, without the consent of the author(s) and/or copyright holder(s), unless the work is under an open content license such as Creative Commons.

**Takedown policy**

Please contact us and provide details if you believe this document breaches copyrights. We will remove access to the work immediately and investigate your claim.



## Effect of truncating electrostatic interactions on predicting thermodynamic properties of water–methanol systems

A. Rahbari, R. Hens, S. H. Jamali, M. Ramdin, D. Dubbeldam & T. J. H. Vlugt

To cite this article: A. Rahbari, R. Hens, S. H. Jamali, M. Ramdin, D. Dubbeldam & T. J. H. Vlugt (2018): Effect of truncating electrostatic interactions on predicting thermodynamic properties of water–methanol systems, *Molecular Simulation*, DOI: [10.1080/08927022.2018.1547824](https://doi.org/10.1080/08927022.2018.1547824)

To link to this article: <https://doi.org/10.1080/08927022.2018.1547824>



© 2018 The Author(s). Published by Informa UK Limited, trading as Taylor & Francis Group



[View supplementary material](#)



Published online: 28 Nov 2018.



[Submit your article to this journal](#)



Article views: 138



[View Crossmark data](#)

# Effect of truncating electrostatic interactions on predicting thermodynamic properties of water–methanol systems

A. Rahbari <sup>a</sup>, R. Hens <sup>a</sup>, S. H. Jamali <sup>a</sup>, M. Ramdin <sup>a</sup>, D. Dubbeldam <sup>b</sup> and T. J. H. Vlugt <sup>a</sup>

<sup>a</sup>Engineering Thermodynamics, Process & Energy Department, Faculty of Mechanical, Maritime and Materials Engineering, Delft, Netherlands;

<sup>b</sup>Van 't Hoff Institute for Molecular Sciences, University of Amsterdam, Amsterdam, Netherlands

## ABSTRACT

The combination of the TraPPE and OPLS/2016 force fields with five water models, TIP3P, SPC/E, OPC, TIP4P/2005 and TIP4P/EW was used to compute mixing enthalpies, excess chemical potentials and activity coefficients of water and methanol. Excess chemical potentials and activity coefficients were computed in an expanded version of the NPT ensemble. We found the best agreement between experimental data for all the computed properties of water–methanol mixtures for the TIP4P/2005–TraPPE force fields. The performance of the spherical cutoff methods in MC and MD simulations was compared to the Ewald summation. The radial distribution functions obtained from the Ewald summation and the Damped-Shifted Force (DSF) method were in excellent agreement. Numerical artifacts appeared at the cutoff radius when the original Wolf method was used to calculate the electrostatic interactions. The calculated excess mixing enthalpies, excess chemical potentials, and activity coefficients of water and methanol obtained from the Wolf method were in good agreement with the DSF method. Our simulation results show that the numerical artifacts of the original Wolf method have little effect for energy calculations in aqueous methanol mixtures.

## ARTICLE HISTORY

Received 29 August 2018  
Accepted 6 November 2018

## KEYWORDS

Water; water–methanol mixtures; wolf method; electrostatics; chemical potential; activity coefficients; excess enthalpy of mixing

## 1. Introduction

Water is one of the most important molecules in science [1,2], central to life, and probably the most studied molecule in the field of molecular simulation [3–7]. From a chemistry perspective, it is a simple molecule formed by two hydrogen atoms and one oxygen atom. The liquid phase has unique properties and complex behaviour [5,8–10]. To date, our understanding of intermolecular and intramolecular interactions of water is far from complete [4,5]. To reproduce different thermophysical properties of water, numerous theoretical and computational models for water were developed and published [3,6,11–13]. In the last decades, due to exponential increase in computational power, molecular simulations are used to compute many properties of water [4–6] in biomolecular [14,15], chemical and industrial applications [12,13,16]. The performance of different water models used to describe the intermolecular interactions are reported extensively in literature [4,17], and is central for predicting properties of water and reproducing experimental data. Since water models are usually fitted to a limited set of experimental data, no water model can simultaneously reproduce all thermophysical properties in good agreement with experiments [4–6]. Therefore, reproducing thermophysical properties of water depends strongly on the choice of experimental data used to fit the intermolecular interaction parameters [17]. Deviations from experimental data may also arise because of inherent limitations in the molecule models of water [3,5,6,18].

Water is a flexible and polarisable molecule [11,19,20]. This means that the electronic structure of the water molecule undergoes deformation due to the electric field induced by the surrounding water or other polar molecules [21]. To account for polarisation effects in the recent years, polarisable force fields for water have been developed [11,20–28]. Some properties of water, such as vapour pressure, critical properties, dielectric constant, and virial coefficient are most accurately predicted by considering polarisation effects [20]. However, the performance of different polarisable force fields to compute chemical potentials and activity coefficients of water is not fully investigated in literature.

Although the water molecule is flexible and polarisable [11], including polarisation effects in MC simulations significantly increases the computational costs [29–31]. In many studies, water is considered as an explicit solvent/medium and is not the main focus. Therefore, the majority of water models in literature are rigid with point charges, and polarisation is ignored [4–6,11]. These simplified models for water are computationally advantageous and the reproduced bulk properties of water are usually in good agreement with experiments at ambient conditions [4,11]. The most popular classical force fields of water include three-point site interaction models [32–34], four-point interaction site models [5], five-point interaction site models [35,36], and six-point interaction site models [8,37]. Many studies compared the performance of different

**CONTACT** T. J. H. Vlugt  t.j.h.vlugt@tudelft.nl

 Supplemental data for this article can be accessed at <http://dx.doi.org/10.1080/08927022.2018.1547824>.

© 2018 The Author(s). Published by Informa UK Limited, trading as Taylor & Francis Group

This is an Open Access article distributed under the terms of the Creative Commons Attribution-NonCommercial-NoDerivatives License (<http://creativecommons.org/licenses/by-nc-nd/4.0/>), which permits non-commercial re-use, distribution, and reproduction in any medium, provided the original work is properly cited, and is not altered, transformed, or built upon in any way.

interaction potentials for predicting thermophysical properties of pure water [5,6].

Aqueous mixtures of methanol are investigated frequently in academia [38–57] and are of practical importance in industrial applications [58–66]. Depending on the application, different mixture properties are required for process design. To compute the mixture properties at different conditions, different force field combinations of water and methanol are considered in few molecular simulation studies [7,38,39,41–45,53,57]. To the best of our knowledge, chemical potentials and activity coefficients of water and methanol are not reported in molecular simulation studies for different/recent force field combinations of water and methanol. Because of the low vapour pressures of water and methanol at ambient conditions, it is also experimentally challenging to determine the activity coefficients.

The most commonly used method to compute the chemical potential in molecular simulation is the well-known Widom’s Test Particle Insertion (WTPI) method [67–69]. In this method, the chemical potential of a component is determined by sampling the interaction energy of a test molecule, inserted at a randomly selected position. Successful sampling of the chemical potential depends strongly on frequent occurrence of spontaneous cavities in the system large enough to accommodate the test molecules [70–72]. Due to the high density of aqueous methanol mixtures at ambient conditions, these spontaneous cavities occur rarely, rendering the WTPI method practically useless [70]. Therefore, advanced simulation techniques are required to compute chemical potentials and activity coefficients in aqueous methanol mixtures [57,67,68,70,71,73–79]. Here, we investigate the performance of different combinations of water and methanol force fields for the computation of chemical potentials and activity coefficients, using state of the art molecular simulation techniques, based on the idea of expanded ensembles [76–78,80].

We focus on popular rigid non-polarisable water models of water. Popular force fields used for water include: TIP3P [33], SPC/E [34], OPC [81], TIP4P/2005 [17], and TIP4P/EW [82]. These models are frequently used in benchmark studies [3–6]. In this study, we have chosen for the TraPPE [83] and OPLS/2016 [84] force fields as the TraPPE force field is widely used, and the OPLS/2016 force field is recently published. The OPLS/2016 force field is claimed to be a more accurate force field for methanol [84]. The force fields for methanol are rigid and non-polarisable. These models are different in bond geometries and/or point charge distributions, and predicting different properties of the mixture depends on different combinations of these force fields [39,40]. The potential energy of the system of rigid molecules with point charges is the sum of pairwise interaction potentials consisting of Lennard–Jones (LJ) and Coulombic interactions:

$$E = \frac{1}{2} \sum_i \sum_{j \neq i} \left[ 4\epsilon_{ij} \left[ \left( \frac{\sigma_{ij}}{r_{ij}} \right)^{12} - \left( \frac{\sigma_{ij}}{r_{ij}} \right)^6 \right] + \frac{1}{4\pi\epsilon_0} \frac{q_i q_j}{r_{ij}} \right], \quad (1)$$

where  $r_{ij}$  where the double summation is over all the interaction sites.  $r_{ij}$  is the distance between atoms  $i$  and  $j$ ,  $\epsilon_0$  is

the dielectric constant,  $q_i$  is the partial charge of atom  $i$ ,  $\sigma_{ij}$  and  $\epsilon_{ij}$  are the LJ parameters between atoms  $i$  and  $j$ , obtained from  $\sigma_i$ ,  $\sigma_j$ ,  $\epsilon_i$  and  $\epsilon_j$ . Proper treatment of LJ and Coulombic interactions are essential for an accurate description of molecular structure, and thermodynamic properties of water and methanol [69,85–93].

In molecular simulation, periodic boundary conditions are applied to simulate bulk phases and compute structural and thermodynamic properties [69]. In systems with periodic boundary conditions, the long-range electrostatic interactions decay slowly with  $r^{-1}$ , and the treatment of the electrostatic interactions becomes computationally demanding. Direct summation of Coulombic interactions is conditionally convergent which means that the results depend on the order of summation [86,94]. Various molecular simulation studies investigated the accuracy and scalability of different methods for treating long-range Coulombic interactions [87,95,96]. These methods can be divided into Ewald-based and cutoff-based methods. In this paper, we investigate to what extent different electrostatic methods influence thermophysical properties of water–methanol mixtures, and whether numerical artifacts are observed. A brief description on electrostatic methods is provided below.

The Ewald summation [69,86,87,92,97] is the most widely used and accepted method to compute electrostatic interactions in molecular simulation and scales as  $\mathcal{O}(N^2)$ . In the Ewald summation, the electrostatic interactions are split into effective short-range interactions, evaluated in real space, and a Fourier series to account for the long-range contribution of the electrostatic interactions, evaluated in reciprocal space [69,86,88,92]. The high computational costs of the Ewald summation have led to efforts to develop faster alternatives [88,90,93,94,96,98]. In the past decades, more Ewald-based algorithms have been developed to reduce the time complexity to  $\mathcal{O}(N \log N)$  by optimising the reciprocal space summation [99,100]. Particle mesh algorithms such as Staggered Mesh Ewald method (StEM) [99], Particle-Particle Particle-Mesh (PPPM) [101], and Particle-Mesh Ewald (PME) [100] are based on the Ewald method and scale as  $\mathcal{O}(N \log N)$  [87,102]. These algorithms allow efficient parallel implementations, and are especially advantageous to use in MD simulations [87]. When the Ewald summation is used in Monte Carlo (MC) simulations, one only need consider the charged atoms that are changed in a trial move. This can be achieved by storing the Fourier part in memory in an efficient way [94]. For a faster computation of the electrostatic interactions, truncation or spherical cutoff-based methods are proposed as an alternative to the Ewald-type methods [89,90,96,103–105].

Cutoff-based methods are based on the idea that the effective electrostatic potential of condensed phases has rather short-ranged behaviour [89,90,93,94,96,98,106,107], and the effect of the long range interactions beyond the cutoff radius becomes negligible due to the screening of charges [87,89,98,104,108]. In the gas phase, the screening of charges is weak compared to the liquid phase [89,90,93,98]. Compared to the Ewald-type methods, the cutoff-based methods are much simpler to implement and scale as  $\mathcal{O}(N)$ . The performance of the

cutoff-based methods are promising especially for bulk homogeneous systems, while in systems with an interface, severe numerical problems may be expected [88]. A common criticism about cutoff-based methods is that numerical artifacts may arise due to the truncation of long-range interactions [87,88,95,109–111]. These numerical artifacts can affect the structure of the liquid. For example, two atoms of opposite charges (positive-negative) prefer to be located within the cutoff radius, while two atoms with the same charge (positive-positive or negative-negative) are preferentially located outside the cutoff radius. As the concept of using a cutoff radius for electrostatic interactions is due to simulation efficiency reasons rather than a physical effect, changes in the liquid structure due to an imposed cutoff radius are non-physical and should be avoided. To observe whether anomalies occur in the liquid structure, the Radial Distribution Function (RDF) of the liquid can be studied. Depending on the extent of the numerical artifacts, energy calculations are affected. Mark et al. reported artificial structuring of water when using atom-based cutoff methods developed by Steinbach et al. [104] to compute the electrostatic interactions [108]. The slow convergence issue appeared especially in truncation and shifting schemes in which the truncation sphere inside the cutoff was not electroneutral [87,90,91]. Wolf et al. realised that the error in computing the electrostatic interactions was related to the net charge inside the cutoff sphere and enforced charge neutrality within the cutoff radius [88,90]. By using a charge-neutralised damped pair potential, fast convergence is achieved and effects of possible artifacts due to the truncation of electrostatic interactions are minimised [88–91,98].

Using the so-called Wolf method, the damped shifted pairwise electrostatic potential for a system of  $N$  charges is obtained from [90,93,94,98]

$$E^{\text{Wolf}} = \frac{1}{2} \sum_{i=1}^N \sum_{\substack{j=1 \\ j \neq i \\ r_{ij} < R_c}}^N q_i q_j \left[ \frac{\text{erfc}(\alpha r_{ij})}{r_{ij}} - \frac{\text{erfc}(\alpha R_c)}{R_c} \right] - \left[ \frac{\text{erfc}(\alpha R_c)}{2R_c} + \frac{\alpha}{\sqrt{\pi}} \right] \sum_{i=1}^N q_i^2, \quad (2)$$

where  $r_{ij}$  is the distance between the partial charges  $i$  and  $j$ ,  $\text{erfc}(x) = 1 - \text{erf}(x)$  is the complementary error function. In principle, other damping functions may be used [85,90].  $R_c$  is the cutoff radius,  $\alpha$  is the Wolf damping parameter, and its value determines how fast the complementary error function approaches zero with increasing  $r_{ij}$ . The second term on the right-hand side of Equation (2) is the energy associated with the so-called self term [90,98]. The Wolf method has been used in different studies including water and ionic systems [96,112–114]. For a nice and readable derivation of the Wolf method for molecular systems, the reader is referred to the paper by Waibel and Gross [98]. Applying the Wolf method to a molecular system, the charge-charge interactions within each molecule should be excluded from the total sum of the electrostatic energy [98] because these are not part of intermolecular interactions. Initially, we consider a system without intramolecular Coulombic interactions, e.g. for rigid molecules.

The total electrostatic energy equals [93,94,115]:

$$E^{\text{Wolf}} = \frac{1}{2} \sum_{i=1}^{N_m} \sum_{a=1}^{N_a^i} \sum_{\substack{j=1 \\ j \neq i \\ r_{iajb} < R_c}}^{N_m} \sum_{b=1}^{N_b^j} q_{ia} q_{jb} \left[ \frac{\text{erfc}(\alpha r_{iajb})}{r_{iajb}} - \frac{\text{erfc}(\alpha R_c)}{R_c} \right] + \frac{1}{2} \sum_{i=1}^{N_m} \sum_{a=1}^{N_a^i} \sum_{\substack{b=1 \\ b \neq a \\ r_{iaib} < R_c}}^{N_a^i} q_{ia} q_{ib} \left[ \frac{\text{erfc}(\alpha r_{iaib})}{r_{iaib}} - \frac{\text{erfc}(\alpha R_c)}{R_c} \right] - \frac{1}{2} \sum_{i=1}^{N_m} \sum_{a=1}^{N_a^i} \sum_{\substack{b=1 \\ b \neq a}}^{N_a^i} \frac{q_{ia} q_{ib}}{r_{iaib}} - \left[ \frac{\text{erfc}(\alpha R_c)}{2R_c} + \frac{\alpha}{\sqrt{\pi}} \right] \sum_{i=1}^{N_m} \sum_{a=1}^{N_a^i} q_{ia}^2. \quad (3)$$

In Equation (3),  $N_m$  is the number of molecules,  $N_a^i$  is the number of atoms in molecule  $i$ , indices  $i$  and  $j$  are used to count the number of molecules, indices  $a$  and  $b$  are used to count atoms within molecules.  $q_{ia}$  is the partial charge of atom  $a$  in molecule  $i$ ,  $r_{iajb}$  is the distance between interaction sites  $a$  and  $b$ . The first and second terms on the right-hand side of Equation (3) are used to compute the pairwise electrostatic interactions between all partial charges in the system, which are screened electrostatic interactions between different molecules and electrostatic interactions inside molecules, respectively. For rigid molecules, we are only interested in intermolecular interactions, and therefore we have to exclude electrostatic interactions within molecules, i.e. charge-charge interactions between the atoms within the molecules. This is achieved by the third term on the right-hand side of Equation (3), the so-called exclusion term, similar to the exclusion term in the Ewald summation [116]. The fourth term on the right-hand side of Equation (3) is the self-interaction term which is similar to that of an atomic system equation (2). For non-rigid molecules, the intramolecular Coulombic interactions should be added to Equation (3) by:

$$E_{\text{Intra}} = \frac{1}{2} \sum_{i=1}^{N_m} \sum_{a=1}^{N_a^i} \sum_{\substack{b=1 \\ b \neq a}}^{N_a^i} c_{ab} \frac{q_{ia} q_{ib}}{r_{iaib}} \quad (4)$$

in which  $c_{ab}$  is a scaling parameter for electrostatic interactions between atom  $a$  and atom  $b$ .  $c_{ab}$  equals zero if atoms  $a$  and  $b$  do not have any intramolecular electrostatic interactions. Several force fields have intramolecular interactions that are scaled [117–121], so the value of  $c_{ab}$  can be non-integer. Note that a cutoff radius is not applied for the intramolecular interactions of Equation (4), and that these interactions are not screened with a  $\text{erfc}(\alpha r)/r$  term. The reason is that for a system consisting of an isolated molecule with intramolecular interactions but no intermolecular interactions, the correct result is obtained, i.e. a direct pairwise  $1/r$  summation over the intramolecular Coulombic interactions. It is important to note that in sharp contrast to the terms for intramolecular Coulombic interactions and intramolecular Coulombic exclusions proposed by Gross et al. [98], in this work no cutoff is imposed for these interactions. It is



expected that this avoids potential artifacts for systems including molecules larger than the cutoff radius.

Fennell and Gezelter [89] found that the damped shifted potential proposed by Wolf et al. (Equation (3)), results in force discontinuity at the cutoff radius in MD simulations. This is undesirable as it may lead to energy drifts [69]. To remove this discontinuity, the electrostatic potential proposed by Fennell and Gezelter (the so-called Damped-Shifted Force (DSF) method) is calculated using

$$\begin{aligned}
 E^{\text{DSF}} = & \frac{1}{2} \sum_{i=1}^{N_m} \sum_{a=1}^{N_a^i} \sum_{\substack{j=1 \\ j \neq i}}^{N_m} \sum_{b=1}^{N_a^j} q_{ia} q_{jb} \left[ \frac{\text{erfc}(\alpha r_{iajb})}{r_{iajb}} - \frac{\text{erfc}(\alpha R_c)}{R_c} \right. \\
 & \left. + \left( \frac{\text{erfc}(\alpha R_c)}{R_c^2} + \frac{2\alpha \exp(-\alpha^2 R_c^2)}{\sqrt{\pi} R_c} \right) (r_{iajb} - R_c) \right] \\
 & + \frac{1}{2} \sum_{i=1}^{N_m} \sum_{a=1}^{N_a^i} \sum_{\substack{b=1 \\ b \neq a}}^{N_a^i} q_{ia} q_{ib} \left[ \frac{\text{erfc}(\alpha r_{iaib})}{r_{iaib}} - \frac{\text{erfc}(\alpha R_c)}{R_c} \right] \\
 & - \frac{1}{2} \sum_{i=1}^{N_m} \sum_{a=1}^{N_a^i} \sum_{\substack{b=1 \\ b \neq a}}^{N_a^i} \frac{q_{ia} q_{ib}}{r_{iaib}} \\
 & - \left[ \frac{\text{erfc}(\alpha R_c)}{2R_c} + \frac{\alpha}{\sqrt{\pi}} \right] \sum_{i=1}^{N_m} \sum_{a=1}^{N_a^i} q_{ia}^2.
 \end{aligned} \tag{5}$$

Similar to Equation (3), the intramolecular Coulombic interactions are not included here, and these interactions need to be taken into account according to Equation (4). For simplicity, Equations (3)–(5) are formulated for single-component systems. Extending these equations to multicomponent systems is trivial: (1) The summation in the first terms of Equations (3) and (5) should be over all intermolecular interactions between all the atoms of all molecules; (2) the summations in other terms of Equations (3) and (5) (and the summation in Equation (4)) should be over all molecules. The extra term on the right-hand side of Equation (5) compared to Equation (3) makes both the potential and its first derivative (the force) continuous at the cutoff radius [89]. Although the continuity of the force at the cutoff radius is of primary interest in MD simulations, the electrostatic potential derived in Equation (5) is slightly different compared to the original Wolf method. This small difference in the electrostatic interaction potential can potentially change the computed structure and/or other properties of the system. In different studies of ionic liquids [89,100,122–124], it was found that the electrostatic energies and forces obtained using the DSF method are in excellent agreement with the conventional Ewald/smooth PME method.

Instead of using an atom-based spherical cutoff method, one could also apply a group-based or charge-group cutoff method [87,89,104]. In this method, atoms are assigned to charge-neutral groups. If the distance between the geometric centres of the charge-neutral groups is smaller than a certain cutoff, all atoms belonging to the charge-neutral groups interact, otherwise no atomic interaction between the two groups is taken into account. Therefore the computational time is reduced by

ignoring the pairwise electrostatic interactions between charge-neutral groups which are further away from the cutoff radius. Another advantage is that the leading  $1/r$  term for Coulombic interactions reduces to a higher order term that decays faster [104]. Gross et al. [98] found no differences between a group-based cutoff radius and an atom-based cutoff radius for the Wolf method, and therefore we have not considered this further in this paper.

This paper is organised as follows. In Section 2, expressions to compute the following thermodynamic properties: excess mixing enthalpy, chemical potentials and activity coefficients are described. Simulation details, force field parameters, and scaling of the intramolecular interactions are described in Section 3. Our simulation results are presented in Section 4. It is shown that the liquid structure obtained using the Wolf method, Equation (3), and the DSF method, Equation (5), is different especially near the cutoff radius. However, computing the excess chemical potentials of water and methanol obtained using the Wolf method and the DSF method yield very similar results. It is also shown that the activity coefficients of water and methanol in water–methanol mixtures computed based on TIP4P/2005 and TraPPE force fields show the best agreement with experimental data. Our conclusions are summarised in Section 5.

## 2. Theory

The enthalpy of a system (pure component or a mixture) can be directly computed from simulations in the  $NPT$  ensemble [69,86]

$$H = \langle U \rangle_{NPT} + P \langle V \rangle_{NPT}, \tag{6}$$

$\langle U \rangle_{NPT}$  is the ensemble average internal energy of the system, and  $\langle V \rangle_{NPT}$  is the ensemble average volume in the  $NPT$  ensemble. For the water–methanol mixture, the excess enthalpy of the mixing is obtained from

$$h_{\text{mix}}^{\text{ex}} = h_{\text{mix}} - (1 - x_{\text{MeOH}})h_{\text{H}_2\text{O}} - x_{\text{MeOH}}h_{\text{MeOH}}, \tag{7}$$

$h^{\text{ex}}$  is the excess enthalpy of mixing with respect to pure liquid,  $h_{\text{mix}}$  is the enthalpy of the water–methanol mixture,  $h_{\text{MeOH}}$  is the enthalpy of pure methanol,  $h_{\text{H}_2\text{O}}$  is the enthalpy of pure water, and  $x_{\text{MeOH}}$  is the mole fraction of methanol. The most common method to compute the chemical potential of a component is the WTPI method [67,68]. Because of inefficient sampling of the chemical potentials of water and methanol using the WTPI method at low temperatures (298 K) [70,72], the Continuous Fractional Component  $NPT$  (CFCNPT) ensemble is used [73] to compute the chemical potentials. For the general case of a multicomponent mixture in this ensemble, the  $NPT$  ensemble is expanded with a fractional molecule of component A, as opposed to all other molecules which are referred to as ‘whole molecules’. For the complete expression of the partition function of this expanded  $NPT$  ensemble, the reader is referred to Ref. [73]. The interaction of the fractional molecule is scaled with a coupling parameter  $\lambda_A \in [0,1]$ . For  $\lambda_A = 0$ , the fractional molecule does not interact with other molecules in the systems, and for  $\lambda_A = 1$  the fractional molecule is fully interacting with the rest of the

molecules in the system, and thus acts as a ‘whole’ molecule. In our previous work, we have shown that the chemical potential of component A in the CFCNPT ensemble is obtained according to [72,73]

$$\mu_A = -\frac{1}{\beta} \ln \left( \frac{\langle V \rangle_{\text{CFCNPT}}}{\Lambda_A^3 (N_A + 1)} \right) - \frac{1}{\beta} \ln \left( \frac{p(\lambda_A \uparrow 1)}{p(\lambda_A \downarrow 0)} \right), \quad (8)$$

$\mu_A$  is the chemical potential of component A,  $\beta = 1/(k_B T)$ , and  $k_B$  is the Boltzmann constant.  $\langle V \rangle_{\text{CFCNPT}}$  is the ensemble average volume in the CFCNPT ensemble,  $\Lambda_A$  is the thermal wavelength,  $N_A$  is the number of whole molecules of type A,  $p(\lambda_A \downarrow 0)$  is the probability of  $\lambda_A$  approaching zero, and  $p(\lambda_A \uparrow 1)$  is the probability of  $\lambda_A$  approaching one. The second term in Equation (8) is the excess chemical potential of component A (with respect to the ideal gas phase). In [73], we show that the WTPI method fails to compute the excess chemical potential of pure water and methanol at ambient conditions. The activity coefficient of component A,  $\gamma_A$ , in a mixture is obtained according to [125,126]

$$\gamma_A = \frac{\rho_A}{x_A \rho_{0A}} \cdot \exp[\beta(\mu_A^{\text{ex}} - \mu_{0A}^{\text{ex}})], \quad (9)$$

$\rho_A$  and  $\rho_{0A}$  are the number densities of component A in the mixture and the reference number density of the pure solvent, respectively.  $\mu_A^{\text{ex}}$  is the excess chemical potential of component A in a mixture with mole fraction of  $x_A$ , and  $\mu_{0A}^{\text{ex}}$  is the excess chemical potential of A in the pure fluid A.

### 3. Simulation details

#### 3.1. Monte Carlo simulations

Different water–methanol mixtures with compositions ranging from  $x_{\text{MeOH}} = 0$  to  $x_{\text{MeOH}} = 1$  are simulated at  $P=1$  bar and  $T=298$  K, both in the conventional  $NPT$  ensemble [69,86] and the CFCNPT ensemble [73]. All MC simulations were performed using our in-house code which is verified to produce the same results as the RASPA software package [127,128] in various works [93,115]. For water, the TIP3P [32], SPC/E [34], OPC [81], TIP4P/2005 [17], and TIP4P/EW [82] force fields, and for methanol the TraPPE [83] and OPLS/2016 [84] force fields are used. All force field parameters are provided in Tables 1 and 2. All molecules are rigid and the interactions between the molecules only consist of LJ and Coulombic interactions. Periodic boundary conditions were used. LJ potentials were truncated but not shifted, and analytic tail corrections and the Lorentz–Berthelot mixing rules were applied [69,86]. For every mixture composition and every

**Table 2.** Force field parameters for methanol used in this study.

| Force field                         | OPLS/2016 [84] | TraPPE [83] |
|-------------------------------------|----------------|-------------|
| $\epsilon_{\text{OO}}$              | 97.775         | 93.000      |
| $\sigma_{\text{OO}}$                | 3.1659         | 3.0200      |
| $\epsilon_{\text{CH}_3\text{CH}_3}$ | 110.450        | 98.000      |
| $\sigma_{\text{CH}_3\text{CH}_3}$   | 3.6449         | 3.75        |
| $q_{\text{O}}$                      | -0.6544        | -0.70000    |
| $q_{\text{H}}$                      | 0.49980        | 0.43500     |
| $q_{\text{CH}_3}$                   | 0.1546         | 0.2650      |
| $r_{\text{OH}}$                     | 0.9450         | 0.9450      |
| $r_{\text{CH}_3\text{O}}$           | 1.43           | 1.43        |

Notes: All molecules are considered rigid.  $\epsilon$  is reported in units of K,  $\sigma$  and  $r$  are reported in units of Å.

water–methanol force field combination, the Wolf and the DSF methods, Equations (3) and (5), were both used to compute the electrostatic interactions.

To obtain the parameters for the Wolf method for pure water and pure methanol, independent simulations were performed in the  $NVT$  ensemble, using SPC/E [34] and OPLS/2016 [84] force fields, close to the experimental densities at  $T=298$  K [129,130]. For dense liquids such as water and methanol at ambient conditions, it is sufficient to plot Figure 1 for a single configuration [93]. For the single equilibrated configuration, the electrostatic energies were calculated for different values of cutoff radii ranging from  $R_c = 10$  Å to  $R_c = 15$  Å, as a function of  $\alpha$ . The relative difference in electrostatic energies, for water and methanol, were compared to the results obtained from the Ewald summation, and the results are shown in Figure 1. It is shown in Figure 1 that the relative difference between the electrostatic energies between these methods is within 0.5% for the cutoff radii ranging from 10 Å to 15 Å, and  $\alpha$  ranging from  $0.1 \text{ \AA}^{-1}$  to  $0.15 \text{ \AA}^{-1}$ . This means that the results obtained from the Wolf method in this  $(\alpha, R_c)$  range, are consistent with the energetics from the Ewald summation. For all simulations, Wolf parameters,  $R_c$  and  $\alpha$  were set to 14 Å and  $0.12 \text{ \AA}^{-1}$ , respectively, and a cutoff radius of 14 Å was used for LJ interactions. The same parameters were used for the DSF method (Equation (5)).

Simulations in the  $NPT$  ensemble were performed to compute the excess mixing enthalpies of water–methanol mixtures (with respect to pure liquid) based on Equation (7). Simulations in the CFCNPT ensemble were performed to compute the excess chemical potentials of water and methanol (with respect to ideal gas phase) using Equation (8). The activity coefficients of water and methanol were obtained using Equation (9). Each simulation in the  $NPT$  ensemble was carried out with  $10^5$  equilibration cycles and  $4 \times 10^6$  production cycles. In each cycle, the number of MC steps equals the total number of molecules, and trial moves were selected with the following probabilities: 1% volume changes,

**Table 1.** Force field parameters for water used in this study.

| Force field            | TIP3P [32] | SPCE/E [34] | OPC [81] | TIP4P/2005 [17] | TIP4P/EW [82] |
|------------------------|------------|-------------|----------|-----------------|---------------|
| $\epsilon_{\text{OO}}$ | 76.500     | 78.175      | 107.086  | 93.196          | 81.899        |
| $\sigma_{\text{OO}}$   | 3.1506     | 3.1660      | 3.1666   | 3.1589          | 3.1644        |
| $q_{\text{O}}$         | -0.8340    | -0.8476     | -1.3582  | -               | -             |
| $q_{\text{H}}$         | 0.41700    | 0.42380     | 0.67910  | 0.55640         | 0.52422       |
| $q_{\text{L}}$         | -          | -           | -        | -1.11280        | -1.04844      |
| $r_{\text{OH}}$        | 0.9572     | 1.0000      | 0.8724   | 0.9572          | 0.9572        |
| $r_{\text{OL}}$        | -          | -           | 0.1594   | 0.1546          | 0.1250        |

Notes: All molecules are considered rigid.  $\epsilon$  is reported in units of K,  $\sigma$  and  $r$  are reported in units of Å.

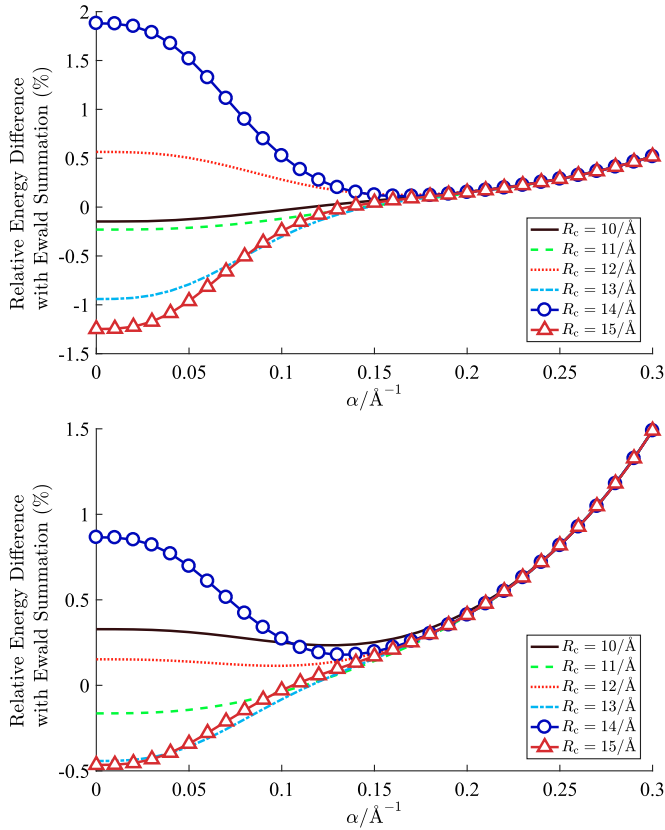


**Figure 1.** (Colour online) Relative differences in computed electrostatic energies between the Wolf method, Equation (3), and the Ewald summation for (a) water and (b) methanol. The parameters for the Ewald summation are calculated based on relative precision of  $10^{-6}$  [93]. The SPC/E [34] and OPLS/2016 [84] force fields were used to obtain the densities of water and methanol at  $T=298$  K and  $P=1$  bar. Individual configurations were obtained at constant densities of  $1000 \text{ kg m}^{-3}$  and  $748 \text{ kg m}^{-3}$  for water and methanol, respectively.

49.5% translations, and 49.5% rotations. Simulations in the CFCNPT ensemble were performed to compute the chemical potentials and activity coefficients of water and methanol at different mixture compositions. To scale the interactions of the fractional molecule in the CFCNPT ensemble, the LJ and Coulombic interactions are decoupled. It is specifically important to switch on the repulsive LJ interactions before the Coulombic interactions, to protect the charges from overlapping [131–136]. Charge-overlaps can potentially lead to huge electrostatic potentials, inaccuracies and numerical instabilities [131–135]. First, the LJ interactions of the fractional molecule are switched on at  $\lambda = 0$  and are fully interacting with the surrounding molecules when  $\lambda$  reaches a certain predefined threshold value of  $\lambda^*$ . Second, the Coulombic interactions of the fractional molecule are switched on at  $\lambda = \lambda^*$  and are fully interacting with the surrounding molecules when  $\lambda = 1$ . In Figure 2, it is shown how the LJ and Coulombic interactions are decoupled and scaled with separate coupling parameters  $\lambda_{\text{LJ}} \in [0,1]$  and  $\lambda_{\text{Coul}} \in [0,1]$  respectively. The precise functional forms for the scaling of the LJ and electrostatic interactions are discussed in Section 3.1.1. Different choices are possible for  $\lambda^*$  depending on the system. Here, we selected  $\lambda^* = 0.8$  and did not attempt to choose the value of  $\lambda^*$  which leads to the most efficient simulation. Note that only the efficiency of the simulation depends on  $\lambda^*$  and not the result.

Beside thermalisation trial moves (translations, rotations, volume changes etc.) [69], three types of trial moves involving

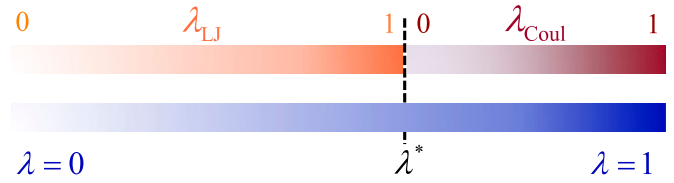


**Figure 2.** (Colour online) Coupling parameter  $\lambda$  to scale the interactions of fractional molecules.  $\lambda_{\text{LJ}} \in [0,1]$  is the coupling parameter used to scale the LJ interactions of the fractional molecule (Equation (10)). At  $\lambda = \lambda^*$ , the Coulombic interactions are switched on.  $\lambda_{\text{Coul}} \in [0,1]$  is the coupling parameter used to scale the Coulombic interactions of the fractional molecule (Equation (11)).

the fractional molecule are used to facilitate gradual particle insertions/removals [73]: (1) Changes in  $\lambda$ : changing the coupling parameter ( $\lambda$ ) of the fractional molecule while keeping the positions of all molecules including the fractional molecule fixed. The trial move is automatically rejected if  $\lambda < 0$  or  $\lambda > 1$  [72,73,115]; (2) Reinsertions: the fractional molecule is moved to a randomly selected position while keeping the value of  $\lambda$  and the positions of all the whole molecules fixed; (3) Identity changes: the fractional molecule is changed into a whole molecule of the same molecule type, and a randomly selected whole molecule of the same type is changed into a fractional molecule. The positions of all molecules and the value of  $\lambda$  are kept fixed in this trial move. These three trial moves are accepted or rejected based on Metropolis acceptance rules [69,115]. Trial moves of type (2) have a high acceptance probability at low values of  $\lambda$ , and trial moves of type (3) has a high acceptance probability only at high values of  $\lambda$  [73,115]. It is possible to define a hybrid trial move in which trial moves of type (2) are only selected at low values of  $\lambda$ , and trial moves of type (3) are only selected at high values of  $\lambda$ . Therefore, trial moves (2) and (3) are only selected when the acceptance probabilities are high. In Refs [73,115], it is shown that such a hybrid trial move obeys detailed balance.

Each simulation in the CFCNPT ensemble was carried out with  $10^5$  equilibration cycles and  $4 \times 10^6$  production cycles. To facilitate the sampling of  $\lambda$ , a weight function ( $W(\lambda)$ ) was used to make the sampled probability of  $\lambda$  flat [77,78]. During equilibration, the Wang-Landau algorithm was used to construct the weight function [137,138]. In each MC step, trial moves were selected with the following probabilities: 1% volume changes, 35% translations, 30% rotations, 17%  $\lambda$  changes, 8.5% reinsertions, and 8.5% identity changes.

### 3.1.1. Scaling of the Lennard–Jones and electrostatic interactions

In CFCNPT simulations, the LJ interactions of the fractional molecule were scaled as follows [77]:

$$u_{\text{LJ}}(r, \lambda_{\text{LJ}}) = \lambda_{\text{LJ}} 4\epsilon \left( \frac{1}{\left[12(1 - \lambda_{\text{LJ}})^2 + (r\sigma)^6\right]^2} - \frac{1}{\left[12(1 - \lambda_{\text{LJ}})^2 + (r\sigma)^6\right]} \right), \quad (10)$$

$\lambda_{\text{LJ}}$  is the coupling parameter for LJ interactions as shown in Figure 2. The Coulombic interactions for the DSF potential



$$\begin{aligned}
E_{\text{Coul}}^{\text{DSF}}(r, \lambda_{\text{Coul}}) &= \frac{1}{2} \sum_{i=1}^{N_m} \sum_{a=1}^{N_a^i} \sum_{\substack{j=1 \\ j \neq i}}^{N_m} \sum_{b=1}^{N_a^j} \lambda_{\text{Coul}} q_{ia} q_{jb} \left[ \frac{\text{erfc}(\alpha[r_{iajb} + r_*])}{r_{iajb} + r_*} - \frac{\text{erfc}(\alpha[R_c + r_*])}{R_c + r_*} \right] \\
&\quad + \left( \frac{\text{erfc}(\alpha[R_c + r_*])}{(R_c + r_*)^2} + \frac{2\alpha \exp(-\alpha^2[R_c + r_*]^2)}{\sqrt{\pi} (R_c + r_*)} \right) (r_{iajb} - R_c) \\
&\quad + \frac{1}{2} \sum_{i=1}^{N_m} \sum_{a=1}^{N_a^i} \sum_{\substack{b=1 \\ b \neq a}}^{N_a^i} \lambda_{\text{Coul}} q_{ia} q_{ib} \left[ \frac{\text{erfc}(\alpha[r_{iaib} + r_*])}{r_{iaib} + r_*} - \frac{\text{erfc}(\alpha[R_c + r_*])}{R_c + r_*} \right] \\
&\quad - \frac{1}{2} \sum_{i=1}^{N_m} \sum_{a=1}^{N_a^i} \sum_{\substack{b=1 \\ b \neq a}}^{N_a^i} \frac{\lambda_{\text{Coul}} q_{ia} q_{ib}}{r_{iaib} + r_*} \\
&\quad - \left[ \frac{\text{erfc}(\alpha R_c)}{2R_c} + \frac{\alpha}{\sqrt{\pi}} \right] \sum_{i=1}^{N_m} \sum_{a=1}^{N_a^i} \lambda_{\text{Coul}} q_{ia}^2,
\end{aligned} \tag{11}$$

are scaled as where  $r_* = A(1 - \lambda_{\text{Coul}})^2$ , and  $A = \frac{1}{2} \text{Å}$ .  $\lambda_{\text{Coul}}$  is the coupling parameter for Coulombic interactions as shown in Figure 2. By ignoring the second line in Equation (11), a similar expression is obtained for the scaled Coulombic interaction of the fractional molecule using the Wolf method (Equation (3)).

### 3.2. Molecular dynamics simulations

All MD simulations were performed with the LAMMPS software package [139]. Periodic boundary conditions were used. All molecules were kept rigid using the SHAKE algorithm [86]. LJ potentials were truncated and analytic tail corrections were applied to compute the energy and pressure of the system [86]. The Lorentz–Berthelot mixing rules were used for non-bonded LJ interactions [69,86]. To compute densities and enthalpies of water–methanol mixtures, MD simulations are performed in the *NPT* ensemble. The Nosé–Hoover thermostat and barostat are used in all MD simulations performed in this work [86]. To calculate the RDFs, the ensemble average densities obtained from *NPT* simulations were used to fix the densities in the *NVT* ensemble simulations. The temperature of the system is regulated by using the Nosé–Hoover thermostat [86]. The length of each simulation for computing thermodynamic properties, i.e. densities and enthalpies, and RDFs in the *NPT* and *NVT* ensembles are 5 ns and 10 ns, respectively. A time step of 1 fs is used to integrate the equations of motion. The specifications of the force fields used in MD simulations are the same as the specifications used in MC simulations. For the Ewald summation method, long-range electrostatic interactions are computed with a relative precision of  $10^{-6}$  [86].

## 4. Results

### 4.1. Electrostatics

The simplest way to characterise the structure of the liquid phase is by calculating its RDF [69,86,140]. To investigate how different methods for handling the electrostatics may

influence the structure of the liquid, a binary mixture of water–methanol (50–50%) was considered as a representative case. The RDF obtained using the Ewald summation, from MD simulations, was considered as a reference case. For this comparison, the TIP4P/2005 [17] and TraPPE [83] force fields were considered. The densities of the binary water–methanol mixtures were obtained from independent MC and MD simulations, based on different treatments of the long-range electrostatic interactions. The relative difference in densities obtained from MD and MC simulations was below 0.2%, see Tables S1, S5 and S15 of the Supporting Information. In Figure 3, three different RDFs are shown for water–water, water–methanol, and methanol–methanol, in a 50–50% water–methanol mixture. The oxygen atoms in water and methanol represent the molecules. Excellent agreement between the RDFs in Figure 3 shows that all electrostatic methods, both in MD and MC simulations can capture the same probability distributions for the first and second coordination shells. The small difference observed at the first coordination shells in Figure 3(a–c) is practically negligible. This can be due to the difference in the computed densities obtained from independent simulations, and/or statistical noise in the simulations [86]. As shown in Figure 3, all the RDFs have converged to unity after distance of 10 Å. For systematic discussion of the RDFs obtained from experiments and molecular simulations, the reader is referred to Refs. [39,41].

In all the RDFs obtained using the Wolf method, a numerical artifact is observed at  $R_c = 14 \text{ Å}$ . This Gaussian-shaped artifact is most noticeable for  $g(\text{O}_{\text{H}_2\text{O}}-\text{O}_{\text{H}_2\text{O}})$  in Figure 3(a), with less than 5% deviation from 1. The artificial structuring at  $R_c = 14 \text{ Å}$  indicates a non-physical behaviour at the cutoff [104,108]. This is due to the discontinuity in intermolecular electrostatic interactions between the molecules inside and outside the cutoff sphere.

To investigate to what extent the numerical artifact of the Wolf method affects the computed thermodynamic properties, excess mixing enthalpies of water–methanol mixtures obtained from MD and MC simulations were compared based on different treatments of electrostatics: the Ewald, DSF and the Wolf

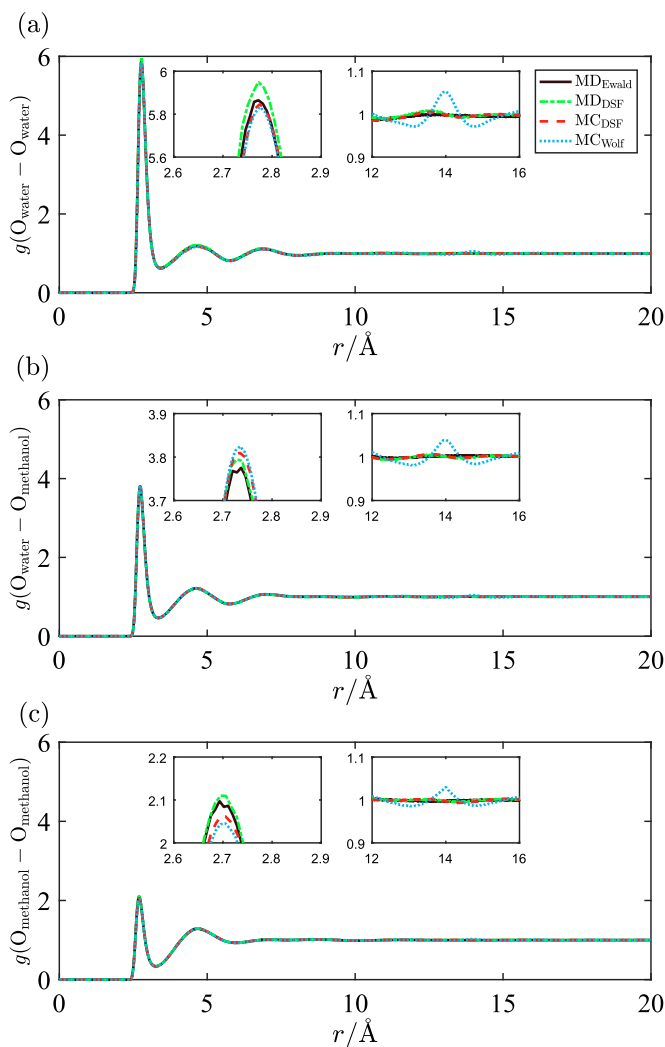


**Figure 3.** (Colour online) Radial distribution functions of water–methanol mixtures (50–50%), at  $T=298$  K and  $P=1$  bar, for: (a) water–water (b) water–methanol (c) methanol–methanol. The TIP4P/2005 [17] and TraPPE [83] force fields were used to compute the density of water–methanol mixtures in MD and MC simulations. The relative difference in densities obtained from MD and MC simulations was 0.2%. To compute the long-range electrostatic interactions, the Ewald and DSF methods were used in MD simulations. In the MC simulations, the Wolf and DSF methods (Equations (3) and (5)) were used.

methods. The water–methanol mixtures were defined based on the TIP4P/2005 [17] and TraPPE [83] force fields. The results are compared in Figure 4. From the MD simulation results, it is clear that the Ewald and DSF methods yield identical excess mixing enthalpies at different mole fractions of methanol,  $x_{\text{MeOH}}$ . Therefore, the excess mixing enthalpies based on the DSF method, from MD simulations, were considered as reference. At  $x_{\text{MeOH}} = 0.9$ , excess mixing enthalpies obtained from MD and MC simulations are equal within statistical uncertainty. At mole fractions  $x_{\text{MeOH}} = 0.5$  and  $x_{\text{MeOH}} = 0.7$ , the computed excess mixing enthalpies using the Wolf method, from MC simulations, are equal, within statistical uncertainty, to those obtained using the DSF method, from MD simulations. At mole fraction  $x_{\text{MeOH}} = 0.3$ , the results using the DSF method, from MC simulations are in excellent agreement with the MD simulation results. Furthermore, the MD and MC simulations yield marginally different results at

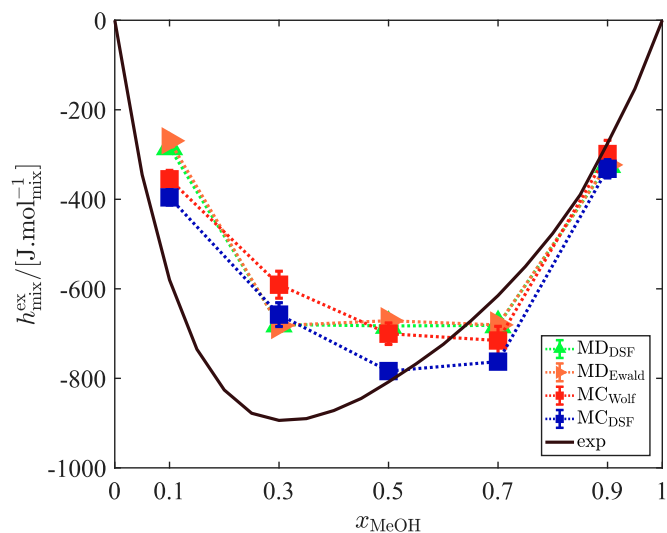


**Figure 4.** (Colour online) Excess enthalpies of mixing for water–methanol mixtures based on the TIP4P/2005 [17] and TraPPE [83] force fields at  $T=298$  K and  $P=1$  bar. To compute the electrostatic energies, the DSF and Ewald [92] methods were used in MD simulations. In MC simulations, the Wolf and DSF methods (Equations (3) and (5)) were used to treat the electrostatic interactions. The solid line indicates experimental values for the excess mixing enthalpy [49]. Dotted lines are a guide to the eye. Error bars are smaller than symbol sizes. Raw data are listed in Tables S1, S5 and S15 of the Supporting Information.

$x_{\text{MeOH}} = 0.1$  and identical results at  $x_{\text{MeOH}} = 0.9$ . This means that there is no clear distinction between the Wolf and DSF methods in calculating excess mixing enthalpies of water–methanol mixtures.

To further investigate the numerical artifact of the Wolf method, excess chemical potentials and activity coefficients of water and methanol are computed using the Wolf and DSF methods, in MC simulations. The experimental values for activity coefficients of water and methanol are taken from Ref. [141]. Experimental excess chemical potentials of water and methanol,  $\mu^{\text{ex}}$ , at different mole fractions were calculated using Equation (8). The experimental density data are provided in Ref. [56]. The excess chemical potentials of pure water and pure methanol,  $\mu_0^{\text{ex}}$ , were computed from empirical equations of state [142–144], using the REFPROP software [145]. For this comparison, the TIP4P/2005 [17] and TraPPE [83] force fields were used for simulations in the CFCNPT ensemble. The computed chemical potentials and activity coefficients of water and methanol are shown in Figures 5 and 6, respectively. It is important to note that at low concentrations of water and methanol, i.e.  $x_{\text{MeOH}} = 0.1$  and  $0.9$ , larger error bars are observed for the excess chemical potentials. This is due to the smaller number of molecules of one of the species (either water or methanol), limiting the number of identity changes of the fractional molecule. Therefore, the sampling of the excess chemical potential becomes more difficult. Since activity coefficients are computed directly from the excess chemical potentials (Equation (9)), only at low concentrations of water and methanol, the values of the activity coefficients display scatter. Considering larger error bars at low mole fractions, it can be seen that the results from the Wolf and DSF methods are in excellent agreement. This suggests that the artifact of the Wolf method observed in the RDFs has a minor effect on thermodynamic properties of water–methanol mixtures. For the

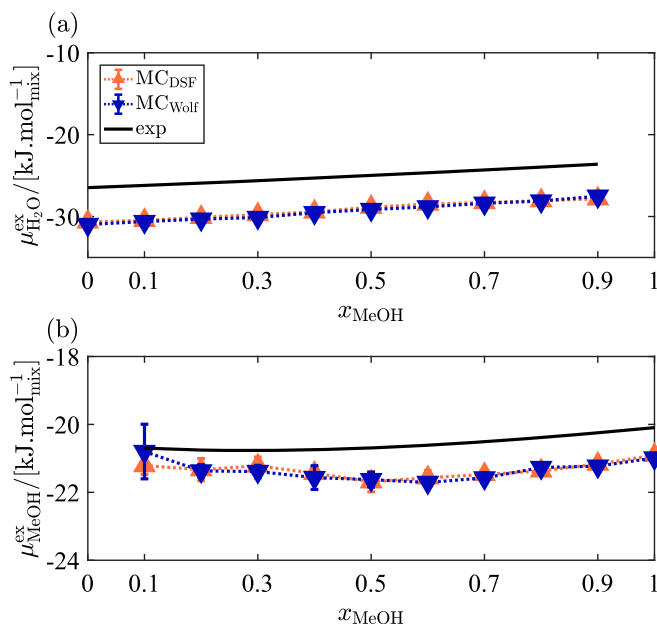


**Figure 5.** (Colour online) Excess chemical potentials of: (a) water, (b) methanol, with respect to the ideal gas phase, in water–methanol mixtures obtained from MC simulations in the CFCNPT ensemble [73], at  $T=298$  K and  $P=1$  bar. The Wolf and the DSF methods (Equations (3) and (5)) were used to calculate the electrostatic interactions. The TIP4P/2005 [17] and TraPPE [83] force fields were used. Error bars are smaller than symbol sizes. Raw data are listed in Tables S5 and S15 of the Supporting Information.

rest of the paper, the results based on the DSF method in MC simulations are presented, and the raw data corresponding to the DSF method are presented in Tables S2 to S11 of The Supporting Information. The results obtained based on the Wolf method, Equation (3) are not considered further in Section 4 due to this artifact. The corresponding properties computed using the Wolf method are listed in Tables S12 to S21 of the Supporting Information.

#### 4.2. Thermodynamic properties of water–methanol mixtures

Few molecular simulation studies investigated the properties of water–methanol mixtures using the OPLS/2016 force field [84] and popular rigid, non-polarisable force fields for water [38–40]. In some cases, non-Lorentz–Berthelot mixing rules [40] were applied to improve the predicted thermodynamic properties of water–methanol compared to experiments. To the best of our knowledge, a comparative analysis of these force field combinations to compute the activity coefficients and excess chemical potentials of water and methanol is missing. To compute the chemical potentials and activity coefficients of water and methanol, TIP3P [32], SPC/E [34], OPC [81], TIP4P/2005 [17], TIP4PEW [82] force fields for water, and the OPLS/2016 [84] and TraPPE [83] force fields for methanol are considered.

The excess mixing enthalpies of water–methanol mixtures were computed for all water–methanol force field combinations, using the DSF method (Equation (5)) to calculate the electrostatic interactions. The results are shown in Figure 7 as a function of  $x_{\text{MeOH}}$ , and the raw data are listed in Tables S2 to S11 of the Supporting Information. From Figure 7, it is clear

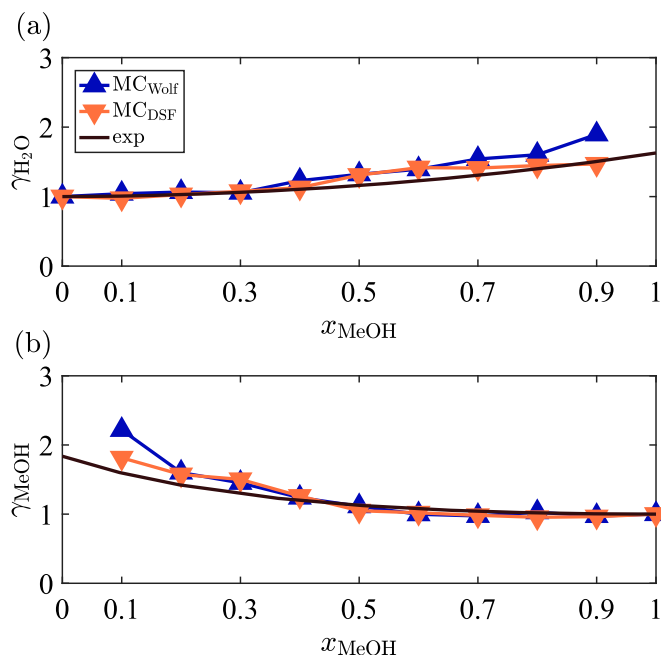


**Figure 6.** (Colour online) Activity coefficients of: (a) water, (b) methanol in water–methanol mixtures obtained from MC simulations in the CFCNPT ensemble, at  $T=298$  K and  $P=1$  bar. The Wolf [90] and the DSF [89] methods were used to calculate the electrostatic interactions. The TIP4P/2005 [17] and TraPPE [83] force fields were used. The line indicates experimental values for the activity coefficients [55]. Raw data are listed in Tables S5 and S15 of the Supporting Information.

that computing the excess mixing enthalpies for water–methanol mixtures using the TraPPE force field for methanol provides considerably better results compared to the OPLS/2016 force field. The sign of the excess mixing enthalpy is predicted correctly and its parabolic shape is reproduced with partial success for all four-site water force fields [39], for  $x_{\text{MeOH}} > 0.5$ . None of the water–methanol force field combinations can precisely reproduce experimental excess enthalpies and the location of the minimum for  $x_{\text{MeOH}} < 0.5$ . Different experimental studies suggest that the unique thermodynamic behaviour of water–methanol mixtures arises from incomplete mixing of the species at molecular level [41,146,147].

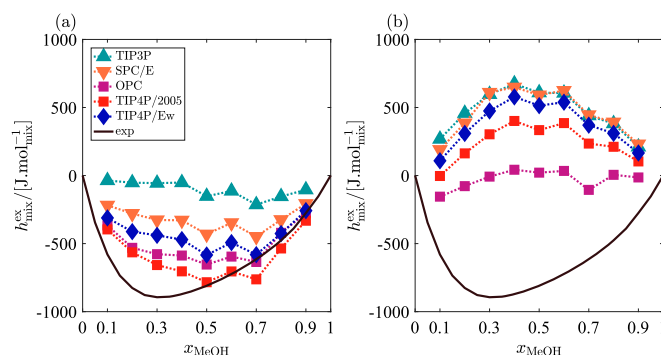


**Figure 7.** (Colour online) Excess mixing enthalpies for water–methanol mixtures defined by: (a) TraPPE [83] and (b) OPLS/2016 [84] force fields at  $T=298$  K and  $P=1$  bar. The TIP3P [33], SPC/E [34], OPC [81], TIP4P/2005 [17], TIP4P/EW [82] force fields were considered for water. The DSF method (Equation (5)) was used to treat the electrostatic interactions. The solid line indicates experimental values for the excess mixing enthalpy [49]. Dotted lines are a guide to the eye. Raw data are listed in Tables S2–S11 of the Supporting Information.

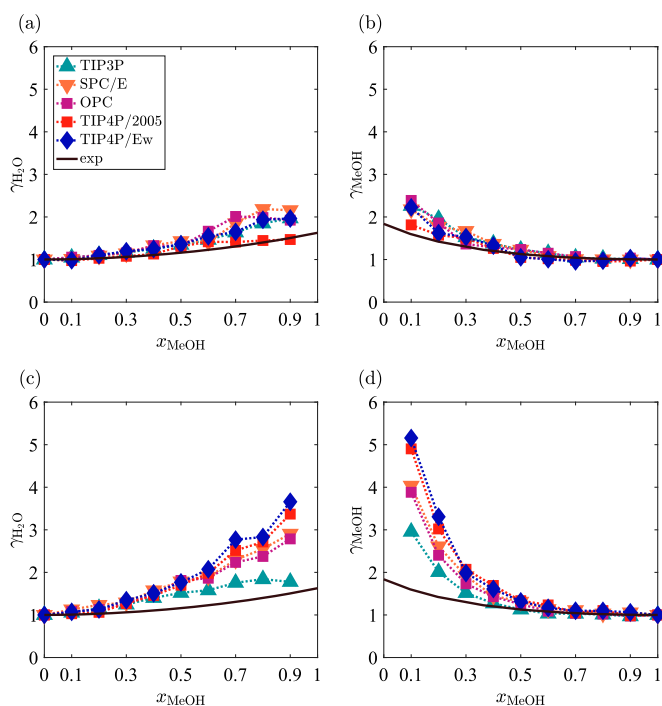


**Figure 8.** (Colour online) Activity coefficients of water and methanol in water–methanol mixtures for different combinations of water–methanol force fields, at  $T=298$  K and  $P=1$  bar. In subfigures (a) and (b); the TraPPE force field was used for methanol and in subfigures (c) and (d); the OPLS/2016 force field was used for methanol. The TIP3P [33], SPC/E [34], OPC [81], TIP4P/2005 [17], TIP4P/EW [82] force fields were considered for water. The DSF method (Equation (5)) was used to treat the electrostatic interactions. The solid lines indicate experimental values for the activity coefficients [55]. Dotted lines are a guide to the eye. Raw data are listed in Tables S2–S11 of the Supporting Information.

Segregation of water and methanol, and formation of clusters, is reported in neutron diffraction experiments [41,146,147] and molecular simulation studies [39] for the whole concentration range. In aqueous methanol solutions, it is observed that hydrophobic methyl groups tend to cluster together, while the hydrophilic hydroxyl groups are pushed further apart and oriented more towards water-rich regions [41]. This leads to a reduction in the extent of the methanol–methanol hydrogen bonding network compared to pure methanol and an addition in the extent of the water–methanol hydrogen bonding network [41,146]. In contrast to methanol, no significant change in the local structure of water is observed in neutron diffraction studies [146]. These observations suggest that water–methanol hydrogen bonding network has a strong influence on the behaviour of the excess properties of water–methanol mixtures. Based on the significant deviation between simulation results and experiments, for  $x_{\text{MeOH}} < 0.5$ , it can be concluded that the selected force field combinations, cannot reproduce the actual clustering/orientation of methanol molecules in aqueous mixtures.

In this work, the TIP4P/2005–TraPPE potential outperforms the other force field combinations in predicting the excess mixing enthalpy and its shape. For water–methanol mixtures defined by the OPLS/2016 force field, the sign of the excess mixing enthalpy is not reproduced, except partially for the OPC–OPLS/2016 potential. A comparative analysis of the TraPPE and OPLS/2016 force field parameters, in Table 2, shows that partial charges on the oxygen and methyl sites are

larger for the TraPPE force field. Similarly, in Table 1, it is shown that the four-site water models have larger partial charges on the oxygen or dummy site. Clearly, increasing partial charges plays an important role in producing the excess molar enthalpies of water–methanol mixtures closer to the experimental values. This is in agreement with the work of Dopazo-Paz et al. [39].

Excess chemical potentials, with respect to the ideal gas phase, and activity coefficients of water and methanol, were calculated using Equations (8) and (9). The results are shown in Figures 8 and 9, and the raw data are listed in Tables S2 to S11 of the Supporting Information. In Figure 8, the computed activity coefficients of water and methanol for all force field combinations were plotted as a function of  $x_{\text{MeOH}}$ . Overall, activity coefficients of methanol obtained based on the OPLS/2016 and TraPPE force fields are in good agreement with the experiments for  $x_{\text{MeOH}} > 0.5$ . For the OPLS/2016 force field, significant deviation from experiments is observed for  $x_{\text{MeOH}} < 0.5$ . In contrast to the OPLS/2016 force field, the computed activity coefficients of methanol for the TraPPE force field are considerably closer to experimental results. For water, the predicted activity coefficients are in good agreement for  $x_{\text{MeOH}} < 0.3$ . The predicted activity coefficients of water in mixtures defined by the OPLS/2016 force field deviate significantly from experimental data for  $x_{\text{MeOH}} > 0.3$ , except for the TIP3P force field. It is clear from Figure 8 that the activity coefficients of different water models, obtained in combination with the TraPPE force field, are in better agreement with the experiments. In Figure 8, it can be seen that the TIP4P2005–TraPPE potential outperforms other force field combinations to predict the activity coefficients closest to the experimental values. Among water–methanol mixtures defined by the OPLS/2016 force field, the activity coefficients obtained from TIP3P–OPLS/2016 force fields deviate less from the experiments.

As the excess chemical potential and activity coefficient are related (Equation (9)), it is important that both properties agree well with experiments. It is expected that the performance of a force field combination should be the same in predicting both the excess chemical potentials and activity coefficients of water and methanol. Since water and methanol force fields are not fitted to experimental chemical potentials, some deviation is expected depending on the force field [70]. In Figure 9, it is shown that all force fields predict the excess chemical potentials with some deviation/shift with respect to the experimental values. Since computing the activity coefficients depends only on the difference between the excess chemical potentials, see Equation (9), a constant shift between the predicted excess chemical potentials and the experimental data does not introduce an error in computing the activity coefficients. This is because term  $(\mu_{\text{A}}^{\text{ex}} - \mu_{\text{0A}}^{\text{ex}})$  in Equation (9) remains constant. This is especially the case for methanol when  $x_{\text{MeOH}} > 0.5$ . For  $x_{\text{MeOH}} < 0.5$ , the calculated excess chemical potentials deviate significantly from the experiments, for methanol OPLS/2016. Clearly, this leads to a considerable error in computing the activity coefficients. It can be seen in Figure 9 that the TIP4P/2005 and TIP3P show the best performance combined with the TraPPE and OPLS/2016 force fields, respectively. For pure components, the excess chemical potential of



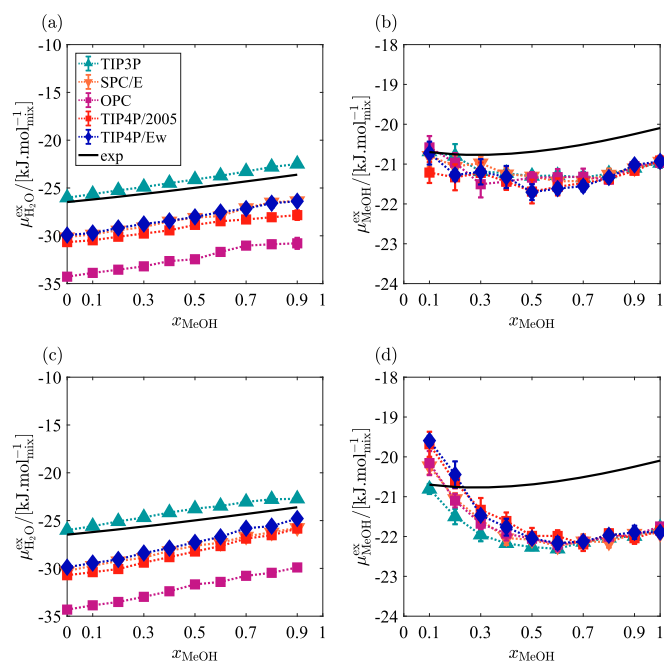


**Figure 9.** (Colour online) Excess chemical potentials of water and methanol, with respect to the ideal gas phase, for different combinations of water–methanol force fields, at  $T=298$  K and  $P=1$  bar. In subfigures (a) and (b); the TraPPE force field was used for methanol and in subfigures (c) and (d); the OPLS/2016 force field was used for methanol. The TIP3P [33], SPC/E [34], OPC [81], TIP4P/2005 [17], TIP4P/EW [82] force fields were considered for water. Error bars are smaller than symbol sizes. The solid lines indicate experimental values for the chemical potentials [142–145]. Dotted lines are a guide to the eye. Raw data are listed in Tables S2–S11 of the Supporting Information.

pure water predicted by the TIP3P force field has the best agreement with the empirical equation of state [144]. The excess chemical potential of water predicted by the OPC force field deviates the most from experimental data. For pure methanol, the computed excess chemical potential using the TraPPE force field agrees best with the experimental equation of state [142,143].

## 5. Conclusions

To predict and reproduce the thermodynamic properties of water, a large number of force fields have been published in literature. The most popular force fields for water are rigid non-polarisable potentials. The performance of these force fields depend on the experimental data used for fitting the force field parameters. These force fields can be combined with other force fields to calculate thermodynamic properties of aqueous solutions. In this work, different force field combinations for water–methanol mixtures were considered to compute excess mixing enthalpies, excess chemical potentials and activity coefficients of water and methanol. In MC simulations, spherical cutoff-based methods are computationally more efficient compared to the Ewald-type methods since computation of electrostatic interactions is reduced to the molecules inside the cutoff sphere. To investigate the accuracy of two spherical cutoff-based methods, i.e. the Wolf and DSF methods (Equations (3) and (5)), RDFs and excess mixing enthalpies of aqueous solutions of methanol were computed and compared to the results obtained from the Ewald summation method.

The RDFs and excess mixing enthalpies obtained from the Ewald summation and DSF methods were in excellent agreement. We observed numerical artifacts at the cutoff radius in RDFs in simulations using the Wolf method. Based on the RDFs, it can be concluded that some orientational correlation exists between the molecules inside and outside the cutoff sphere. This may imply that the dielectric properties of water are not treated correctly [111]. However, the good agreement between the excess mixing enthalpies, activity coefficients, and chemical potentials computed based on the DSF and Wolf methods suggests that these numerical artifacts have a small effect on thermodynamic properties. By using the DSF method, we investigated the performance of the TraPPE and OPLS/2016 force fields for methanol combined with five water models: TIP3P, SPC/E, OPC, TIP4P/2005, and TIP4P/EW. For these force field combinations, we computed excess mixing enthalpies, chemical potentials and activity coefficients of water and methanol. All these properties are reproduced better by the TraPPE force field compared to the OPLS/2016 force field. The predicted properties of water–methanol mixture defined by TIP4P/2005–TraPPE force fields show the best agreement with experimental data compared to other force field combinations.

## Disclosure statement

No potential conflict of interest was reported by the authors.

## Funding

This work was sponsored by NWO Exacte Wetenschappen (Physical Sciences) for the use of supercomputer facilities, with financial support from the Nederlandse Organisatie voor Wetenschappelijk Onderzoek (Netherlands Organization for Scientific Research, NWO). TJHV acknowledges NWO-CW for a VICI grant.

## ORCID

A. Rahbari <http://orcid.org/0000-0002-6474-3028>  
 R. Hens <http://orcid.org/0000-0002-6147-0749>  
 S. H. Jamali <http://orcid.org/0000-0002-4198-0901>  
 M. Ramdin <http://orcid.org/0000-0002-8476-7035>  
 D. Dubbeldam <http://orcid.org/0000-0002-4382-1509>  
 T. J. H. Vlugt <http://orcid.org/0000-0003-3059-8712>

## References

- [1] Poirier J. Rheology of ices: a key to the tectonics of the ice moons of Jupiter and Saturn. *Nature*. 1982;299:683.
- [2] Gallo P, Amann-Winkel K, Angell CA, et al. Water: a tale of two liquids. *Chem Rev*. 2016;116:7463–7500.
- [3] Izadi S, Anandakrishnan R, Onufriev AV. Building water models: a different approach. *J Phys Chem Lett*. 2014;5:3863–3871.
- [4] Onufriev AV, Izadi S. Water models for biomolecular simulations. *WIREs Comput Mol Sci*. 2018;8:e1347.
- [5] Vega C, Abascal JLF. Simulating water with rigid non-polarizable models: a general perspective. *Phys Chem Chem Phys*. 2011;13:19663–19688.
- [6] Guillot B. A reappraisal of what we have learnt during three decades of computer simulations on water. *J Mol Liq*. 2002;101:219–260.



- [7] Jorgensen WL, Chandrasekhar J, Madura JD, et al. Comparison of simple potential functions for simulating liquid water. *J Chem Phys.* 1983;79:926–935.
- [8] Tröster P, Lorenzen K, Tavan P. Polarizable six-point water models from computational and empirical optimization. *J Phys Chem B.* 2014;118:1589–1602.
- [9] Finney JL. The water molecule and its interactions: the interaction between theory, modelling, and experiment. *J Mol Liq.* 2001;90:303–312.
- [10] Ball P. Water as an active constituent in cell biology. *Chem Rev.* 2008;108:74–108.
- [11] Vega C, Abascal JLF, Conde MM, et al. What ice can teach us about water interactions: a critical comparison of the performance of different water models. *Faraday Discuss.* 2009;141:251–276.
- [12] Castillo J, Dubbeldam D, Vlugt TJH, et al. Evaluation of various water models for simulation of adsorption in hydrophobic zeolites. *Mol Simul.* 2009;35:1067–1076.
- [13] Castillo JM, Silvestre-Albero J, Rodriguez-Reinoso F, et al. Water adsorption in hydrophilic zeolites: experiment and simulation. *Phys Chem Chem Phys.* 2013;15:17374–17382.
- [14] Ball P. Water: water – an enduring mystery. *Nature.* 2008;452:291–292.
- [15] Chopra G, Summa CM, Levitt M. Solvent dramatically affects protein structure refinement. *Proc Natl Acad Sci.* 2008;105:20239–20244.
- [16] Rahbari A, Ramdin M, van den Broeke LJP, et al. Combined steam reforming of methane and formic acid to produce syngas with an adjustable H<sub>2</sub>:CO ratio. *Ind Eng Chem Res.* 2018; DOI:10.1021/acscicr8b02443, in press.
- [17] Abascal JLF, Vega C. A general purpose model for the condensed phases of water: TIP4P/2005. *J Chem Phys.* 2005;123:234505.
- [18] Wang LP, Head-Gordon T, Ponder JW, et al. Systematic improvement of a classical molecular model of water. *J Phys Chem B.* 2013;117:9956–9972.
- [19] Halgren TA, Damm W. Polarizable force fields. *Curr Opin Struct Biol.* 2001;11:236–242.
- [20] Jiang H, Moulton OA, Economou IG, et al. Hydrogen-bonding polarizable intermolecular potential model for water. *J Phys Chem B.* 2016;120:12358–12370.
- [21] Gladich I, Roeselov M. Comparison of selected polarizable and nonpolarizable water models in molecular dynamics simulations of ice I<sub>h</sub>. *Phys Chem Chem Phys.* 2012;14:11371–11385.
- [22] Chen B, Xing J, Siepmann JI. Development of polarizable water force fields for phase equilibrium calculations. *J Phys Chem B.* 2000;104:2391–2401.
- [23] Yesylevskyy SO, Schäfer LV, Sengupta D, et al. Polarizable water model for the coarse-grained MARTINI force field. *PLoS Comput Biol.* 2010;116:1–17.
- [24] Kunz APE, van Gunsteren WF. Development of a nonlinear classical polarization model for liquid water and aqueous solutions: COS/D. *J Phys Chem A.* 2009;113:11570–11579.
- [25] Lamoureux G, MacKerell AD, Roux B. A simple polarizable model of water based on classical drude oscillators. *J Chem Phys.* 2003;119:5185–5197.
- [26] Lamoureux G, Harder E, Vorobyov IV, et al. A polarizable model of water for molecular dynamics simulations of biomolecules. *Chem Phys Lett.* 2006;418:245–249.
- [27] Ren P, Ponder JW. Polarizable atomic multipole water model for molecular mechanics simulation. *J Phys Chem B.* 2003;107:5933–5947.
- [28] Laury ML, Wang LP, Pande VS, et al. Revised parameters for the AMOEBA polarizable atomic multipole water model. *J Phys Chem B.* 2015;119:9423–9437.
- [29] Becker TM, Dubbeldam D, Lin LC, et al. Investigating polarization effects of CO<sub>2</sub> adsorption in MgMOF-74. *J Comput Sci.* 2016;15:86–94.
- [30] Antila HS, Salonen E. Polarizable force fields. In: Monticelli L, Salonen E, editors. *Biomolecular simulations: methods and protocols.* Chapter 9. Totowa, NJ: Humana Press; 2013. p. 215–241.
- [31] Rick SW, Stuart SJ. Potentials and algorithms for incorporating polarizability in computer simulations. In: Lipkowitz KB, Salonen DB Boyd, editors. *Reviews in computational chemistry.* Vol. 18; Chapter 3. Hoboken (NJ): Wiley-VCH; 2002. p. 89–146.
- [32] Jorgensen WL, Chandrasekhar J, Madura JD, et al. Comparison of simple potential functions for simulating liquid water. *J Chem Phys.* 1983;79:926–935.
- [33] Mark P, Nilsson L. Structure and dynamics of the TIP3P, SPC, and SPC/E water models at 298 K. *J Phys Chem A.* 2001;105:9954–9960.
- [34] Berendsen HJC, Grigera JR, Straatsma TP. The missing term in effective pair potentials. *J Phys Chem.* 1987;91:6269–6271.
- [35] Mahoney MW, Jorgensen WL. A five-site model for liquid water and the reproduction of the density anomaly by rigid, nonpolarizable potential functions. *J Chem Phys.* 2000;112:8910–8922.
- [36] Rick SW. A reoptimization of the five-site water potential (TIP5P) for use with Ewald sums. *J Chem Phys.* 2004;120:6085–6093.
- [37] Nada H, van der Eerden JPJM. An intermolecular potential model for the simulation of ice and water near the melting point: a six-site model of H<sub>2</sub>O. *J Chem Phys.* 2003;118:7401–7413.
- [38] Martínez-Jiménez M, Saint-Martin H. A four-site molecular model for simulations of liquid methanol and water–methanol mixtures: MeOH-4P. *J Chem Theory Comput.* 2018;14:2526–2537.
- [39] Dopazo-Paz A, Gómez-Álvarez P, González-Salgado D. Thermodynamics and structure of the {water+ methanol} system viewed from three simple additive pair-wise intermolecular potentials based on the rigid molecule approximation. *Collect Czech Chem Commun.* 2010;75:617–635.
- [40] Moučka F, Nezbeda I. Water–methanol mixtures with non-Lorentz-Berthelot combining rules: a feasibility study. *J Mol Liq.* 2011;159:47–51.
- [41] Dougan L, Bates SP, Hargreaves R, et al. Methanol–water solutions: a bi-percolating liquid mixture. *J Chem Phys.* 2004;121:6456–6462.
- [42] Ferrario M, Haughney M, McDonald IR, et al. Molecular-dynamics simulation of aqueous mixtures: methanol, acetone, and ammonia. *J Chem Phys.* 1990;93:5156–5166.
- [43] Mallamace F, Corsaro C, Mallamace D, et al. Dynamical properties of water–methanol solutions. *J Chem Phys.* 2016;144:064506.
- [44] Matsumoto M, Takaoka Y, Kataoka Y. Liquid-vapor interface of water–methanol mixture. I. computer simulation. *J Chem Phys.* 1993;98:1464–1472.
- [45] Wensink EJW, Hoffmann AC, van Maaren PJ, et al. Dynamic properties of water/alcohol mixtures studied by computer simulation. *J Chem Phys.* 2003;119:7308–7317.
- [46] González-Salgado D, Nezbeda I. Excess properties of aqueous mixtures of methanol: simulation versus experiment. *Fluid Phase Equilib.* 2006;240:161–166.
- [47] Wormald C, Badock L, Lloyd M. Excess enthalpies for (water + methanol) at  $T = 423$  K to  $T = 523$  and pressures up to 20 MPa. a new flow mixing calorimeter. *J Chem Thermodyn.* 1996;28:603–613.
- [48] Wormald C, Yerlett T. Molar enthalpy increments for (0.5 H<sub>2</sub>O + 0.5 CH<sub>3</sub>OH) at temperatures up to 573.2 K and pressures up to 13.0 MPa. *J Chem Thermodyn.* 2000;32:97–105.
- [49] Simonson J, Bradley D, Busey R. Excess molar enthalpies and the thermodynamics of (methanol + water) to 573 K and 40 MPa. *J Chem Thermodyn.* 1987;19:479–492.
- [50] Kuroki T, Kagawa N, Endo H, et al. Specific heat capacity at constant volume for water, methanol, and their mixtures at temperatures from 300 K to 400 K and pressures to 20 MPa. *J Chem Eng Data.* 2001;46:1101–1106.
- [51] Xiao C, Bianchi H, Tremaine PR. Excess molar volumes and densities of (methanol+water) at temperatures between 323 K and 573 K and pressures of 7.0 MPa and 13.5 MPa. *J Chem Thermodyn.* 1997;29:261–286.
- [52] Lama R, Lu BCY. Excess thermodynamic properties of aqueous alcohol solutions. *J Chem Eng Data.* 1965;10:216–219.
- [53] Vlček L, Nezbeda I. Excess properties of aqueous mixtures of methanol: simple models versus experiment. *J Mol Liq.* 2007;131–132:158–162.

- [54] Tomaszewicz I, Randzio S, Gierycz P. Excess enthalpy in the methanol–water system at 278.15, 298.15 and 323.15 K under pressures of 0.1, 20 and 39 MPa: II. experimental results and their analytical presentation. *Thermochimica Acta*. 1986;103:281–289.
- [55] Gmehling J, Onken U, Arlt W, et al. Chemistry data series, vapor–liquid equilibrium data collection, vol. 1, part 1c. 1st ed. Frankfurt am Main, Germany: DECHEMA; 1986.
- [56] Mikhail SZ, Kimel WR. Densities and viscosities of methanol–water mixtures. *J Chem Eng Data*. 1961;6:533–537.
- [57] Tanaka H, Gubbins KE. Structure and thermodynamic properties of water–methanol mixtures: role of the water–water interaction. *J Chem Phys*. 1992;97:2626–2634.
- [58] Schrader J, Schilling M, Holtmann D, et al. Methanol-based industrial biotechnology: current status and future perspectives of methylotrophic bacteria. *Trends Biotechnol*. 2009;27:107–115.
- [59] Li X, Faghri A. Review and advances of direct methanol fuel cells (DMFCs) part I: design, fabrication, and testing with high concentration methanol solutions. *J Power Sources*. 2013;226:223–240.
- [60] Olah GA. Beyond oil and gas: the methanol economy. *Angew Chem Int Ed*. 2005;44:2636–2639.
- [61] Hogarth MP, Hards GA. Direct methanol fuel cells. *Platin Met Rev*. 1996;40:150–159.
- [62] Heinzel A, Barragán V. A review of the state-of-the-art of the methanol crossover in direct methanol fuel cells. *J Power Sources*. 1999;84:70–74.
- [63] Aricò AS, Srinivasan S, Antonucci V. Dmfcs: from fundamental aspects to technology development. *Fuel Cells*. 2001;1:133–161.
- [64] Mahmood A, Bano S, Kim SG, et al. Water–methanol separation characteristics of annealed SA/PVA complex membranes. *J Memb Sci*. 2012;415–416:360–367.
- [65] Shah D, Kissick K, Ghorpade A, et al. Pervaporation of alcohol-water and dimethylformamide-water mixtures using hydrophilic zeolite NaA membranes: mechanisms and experimental results. *J Memb Sci*. 2000;179:185–205.
- [66] Winarto A, Takaiwa D, Yamamoto E, et al. Water–methanol separation with carbon nanotubes and electric fields. *Nanoscale*. 2015;7:12659–12665.
- [67] Widom B. Some topics in the theory of fluids. *J Chem Phys*. 1963;39:2808–2812.
- [68] Widom B. Potential-distribution theory and the statistical mechanics of fluids. *J Phys Chem*. 1982;86:869–872.
- [69] Frenkel D, Smit B. Understanding molecular simulation: from algorithms to applications. 2nd ed. San Diego (CA): Academic Press; 2002.
- [70] Rahbari A, Poursaeidesfahani A, Torres-Knoop A, et al. Chemical potentials of water, methanol, carbon dioxide and hydrogen sulphide at low temperatures using continuous fractional component Gibbs ensemble Monte Carlo. *Mol Simul*. 2018;44:405–414.
- [71] Sindzingre P, Ciccotti G, Massobrio C, et al. Partial enthalpies and related quantities in mixtures from computer simulation. *Chem Phys Lett*. 1987;136:35–41.
- [72] Poursaeidesfahani A, Torres-Knoop A, Dubbeldam D, et al. Direct free energy calculation in the continuous fractional component Gibbs ensemble. *J Chem Theory Comput*. 2016;12:1481–1490.
- [73] Rahbari A, Hens R, Nikolaidis IK, et al. Computation of partial molar properties using continuous fractional component Monte Carlo. *Mol Phys*. 2018;116:3331–3344. DOI:10.1080/00268976.2018.1451663.
- [74] Sindzingre P, Massobrio C, Ciccotti G, et al. Calculation of partial enthalpies of an argon-krypton mixture by NPT molecular dynamics. *Chem Phys*. 1989;129:213–224.
- [75] Beutler TC, Mark AE, van Schaik RC, et al. Avoiding singularities and numerical instabilities in free energy calculations based on molecular simulations. *Chem Phys Lett*. 1994;222:529–539.
- [76] Escobedo FA, de Pablo JJ. Expanded grand canonical and Gibbs ensemble Monte Carlo simulation of polymers. *J Chem Phys*. 1996;105:4391–4394.
- [77] Shi W, Maginn EJ. continuous fractional component Monte Carlo: an adaptive biasing method for open system atomistic simulations. *J Chem Theory Comput*. 2007;3:1451–1463.
- [78] Shi W, Maginn EJ. Improvement in molecule exchange efficiency in Gibbs ensemble Monte Carlo: development and implementation of the continuous fractional component move. *J Comput Chem*. 2008;29:2520–2530.
- [79] Kofke DA. Free energy methods in molecular simulation. *Fluid Phase Equilib*. 2005;228–229:41–48.
- [80] Wilding NB, Müller M. Accurate measurements of the chemical potential of polymeric systems by Monte Carlo simulation. *J Chem Phys*. 1994;101:4324–4330.
- [81] Izadi S, Anandkrishnan R, Onufriev AV. Building water models: a different approach. *J Phys Chem Lett*. 2014;5:3863–3871.
- [82] Horn HW, Swope WC, Pitera JW, et al. Development of an improved four-site water model for biomolecular simulations: TIP4P-EW. *J Chem Phys*. 2004;120:9665–9678.
- [83] Chen B, Potoff JJ, Siepmann JI. Monte Carlo calculations for alcohols and their mixtures with alkanes. Transferable potentials for phase equilibria. 5. United-atom description of primary, secondary, and tertiary alcohols. *J Phys Chem B*. 2001;105:3093–3104.
- [84] Gonzalez-Salgado D, Vega C. A new intermolecular potential for simulations of methanol: the OPLS/2016 model. *J Chem Phys*. 2016;145:034508.
- [85] Fanourgakis GS. An extension of Wolf’s method for the treatment of electrostatic interactions: application to liquid water and aqueous solutions. *J Phys Chem B*. 2015;119:1974–1985.
- [86] Allen MP, Tildesley DJ. Computer simulation of liquids. 2nd ed. Oxford: Oxford University Press; 2017.
- [87] Cisneros GA, Karttunen M, Ren P, et al. Classical electrostatics for biomolecular simulations. *Chem Rev*. 2014;114:779–814.
- [88] Fukuda I, Nakamura H. Non-Ewald methods: theory and applications to molecular systems. *Biophys Rev*. 2012;4:161–170.
- [89] Fennell CJ, Gezelter JD. Is the Ewald summation still necessary? Pairwise alternatives to the accepted standard for long-range electrostatics. *J Chem Phys*. 2006;124:234104.
- [90] Wolf D, Keblinski P, Phillpot SR, et al. Exact method for the simulation of Coulombic systems by spherically truncated, pairwise  $r^{-1}$  summation. *J Chem Phys*. 1999;110:8254–8282.
- [91] Wolf D. Reconstruction of NaCl surfaces from a dipolar solution to the Madelung problem. *Phys Rev Lett*. 1992;68:3315–3318.
- [92] Ewald PP. Die Berechnung optischer und elektrostatischer Gitterpotentiale. *Ann Phys*. 1921;369:253–287.
- [93] Hens R, Vlught TJH. Molecular simulation of vapor–liquid equilibria using the Wolf method for electrostatic interactions. *J Chem Eng Data*. 2018;63(4):1096–1102.
- [94] Vlught TJH, García-Pérez E, Dubbeldam D, et al. Computing the heat of adsorption using molecular simulations: the effect of strong Coulombic interactions. *J Chem Theory Comput*. 2008;4:1107–1118.
- [95] Mendoza FN, López-Lemus J, Chapela GA, et al. The Wolf method applied to the liquid–vapor interface of water. *J Chem Phys*. 2008;129:024706.
- [96] McCann BW, Acevedo O. Pairwise alternatives to Ewald summation for calculating long-range electrostatics in ionic liquids. *J Chem Theory Comput*. 2013;9:944–950.
- [97] Toukmaji AY, Board Jr JA. Ewald summation techniques in perspective: a survey. *Comput Phys Commun*. 1996;95:73–92.
- [98] Waibel C, Gross J. Modification of the Wolf method and evaluation for molecular simulation of vapor–liquid equilibria. *J Chem Theory Comput*. 2018;14:2198–2206.
- [99] Cerutti DS, Duke RE, Darden TA, et al. Staggered mesh Ewald: an extension of the smooth particle-mesh Ewald method adding great versatility. *J Chem Theory Comput*. 2009;5:2322–2338.
- [100] Darden T, York D, Pedersen L. Particle mesh Ewald: an  $N \log(N)$  method for Ewald sums in large systems. *J Chem Phys*. 1993;98:10089–10092.
- [101] Neelov A, Holm C. Interlaced P3M algorithm with analytical and ik-differentiation. *J Chem Phys*. 2010;132:234103.

- [102] Isele-Holder RE, Mitchell W, Hammond JR, et al. Reconsidering dispersion potentials: reduced cutoffs in mesh-based Ewald solvers can be faster than truncation. *J Chem Theory Comput.* 2013;9:5412–5420.
- [103] Saito M. Molecular dynamics simulations of proteins in solution: artifacts caused by the cutoff approximation. *J Chem Phys.* 1994;101:4055–4061.
- [104] Steinbach PJ, Brooks BR. New spherical-cutoff methods for long-range forces in macromolecular simulation. *J Comput Chem.* 1994;15:667–683.
- [105] Hansen JS, Schröder TB, Dyre JC. Simplistic Coulomb forces in molecular dynamics: comparing the Wolf and shifted-force approximations. *J Phys Chem B.* 2012;116:5738–5743.
- [106] Levitt M, Hirshberg M, Sharon R, et al. Potential energy function and parameters for simulations of the molecular dynamics of proteins and nucleic acids in solution. *Comput Phys Commun.* 1995;91:215–231.
- [107] Evjen HM. On the stability of certain heteropolar crystals. *Phys Rev.* 1932;39:675–687.
- [108] Pekka M, Lennart N. Structure and dynamics of liquid water with different long-range interaction truncation and temperature control methods in molecular dynamics simulations. *J Comput Chem.* 2002;23:1211–1219.
- [109] Patra M, Karttunen M, Hyvnen M, et al. Molecular dynamics simulations of lipid bilayers: major artifacts due to truncating electrostatic interactions. *Biophys J.* 2003;84:3636–3645.
- [110] van der Spoel D, van Maaren PJ. The origin of layer structure artifacts in simulations of liquid water. *J Chem Theory Comput.* 2006;2:1–11.
- [111] van der Spoel D, van Maaren PJ, Berendsen HJC. A systematic study of water models for molecular simulation: derivation of water models optimized for use with a reaction field. *J Chem Phys.* 1998;108:10220–10230.
- [112] Ghobadi AF, Taghikhani V, Elliott JR. Investigation on the solubility of SO<sub>2</sub> and CO<sub>2</sub> in imidazolium-based ionic liquids using NPT Monte Carlo simulation. *J Phys Chem B.* 2011;115:13599–13607.
- [113] Mahadevan TS, Garofalini SH. Dissociative water potential for molecular dynamics simulations. *J Phys Chem B.* 2007;111:8919–8927.
- [114] Carlos A, Alejandro GV. Monte Carlo simulations of primitive models for ionic systems using the Wolf method. *Mol Phys.* 2006;104:1475–1486.
- [115] Poursaeidesfahani A, Hens R, Rahbari A, et al. Efficient application of continuous fractional component Monte Carlo in the reaction ensemble. *J Chem Theory Comput.* 2017;13:4452–4466.
- [116] Smith W, Forester T, Todorov I, et al. The dl poly 2 user manual. CCLRC, Daresbury Laboratory, Daresbury, Warrington WA4 4AD, England; 2001. 2.
- [117] Cornell WD, Cieplak P, Bayly CI, et al. A second generation force field for the simulation of proteins, nucleic acids, and organic molecules. *J Amer Chem Soc.* 1995;117:5179–5197.
- [118] MacKerell AD, Bashford D, Bellott M, et al. All-atom empirical potential for molecular modeling and dynamics studies of proteins. *J Phys Chem B.* 1998;102:3586–3616.
- [119] Oostenbrink C, Villa A, Mark AE, et al. A biomolecular force field based on the free enthalpy of hydration and solvation: the GROMOS force-field parameter sets 53A5 and 53A6. *J Comput Chem.* 2004;25:1656–1676.
- [120] Jorgensen WL, Maxwell DS, Tirado-Rives J. Development and testing of the OPLS all-atom force field on conformational energetics and properties of organic liquids. *J Amer Chem Soc.* 1996;118:11225–11236.
- [121] Martin MG, Siepmann JI. Transferable potentials for phase equilibria. 1. United-atom description of n-alkanes. *J Phys Chem B.* 1998;102:2569–2577.
- [122] Shi W, Maginn EJ. Atomistic simulation of the absorption of carbon dioxide and water in the ionic liquid 1-n-hexyl-3-methylimidazolium Bis(trifluoromethylsulfonyl)imide ([hmim][Tf<sub>2</sub>n]). *J Phys Chem B.* 2008;112:2045–2055.
- [123] Shi W, Myers CR, Luebke DR, et al. Theoretical and experimental studies of CO<sub>2</sub> and H<sub>2</sub> separation using the 1-Ethyl-3-methylimidazolium acetate ([emim][CH<sub>3</sub>COO]) ionic liquid. *J Phys Chem B.* 2012;116:283–295.
- [124] Shi W, Sorescu DC. Molecular simulations of CO<sub>2</sub> and H<sub>2</sub> sorption into ionic liquid 1-n-Hexyl-3-methylimidazolium Bis(trifluoromethylsulfonyl)amide ([hmim][Tf<sub>2</sub>n]) confined in carbon nanotubes. *J Phys Chem B.* 2010;114:15029–15041.
- [125] Balaji SP, Schnell SK, McGarrity ES, et al. A direct method for calculating thermodynamic factors for liquid mixtures using the permuted Widom test particle insertion method. *Mol Phys.* 2013;111:287–296.
- [126] Hempel S, Fischer J, Paschek D, et al. Activity coefficients of complex molecules by molecular simulation and Gibbs-Duhem integration. *Soft Mater.* 2012;10:26–41.
- [127] Dubbeldam D, Calero S, Ellis DE, RASPA: molecular simulation software for adsorption and diffusion in flexible nanoporous materials. *Mol Simul.* 2015;42:81–101.
- [128] Dubbeldam D, Torres-Knoop A, Walton KS. On the inner workings of Monte Carlo codes. *Mol Simul.* 2013;39:1253–1292.
- [129] Goodwin RD. Methanol thermodynamic properties from 176 to 673 K at pressures to 700 bar. *J Phys Chem Ref Data.* 1987;16:799–892.
- [130] Moran MJ, Shapiro HN. Fundamentals of engineering thermodynamics. 5th ed. West Sussex: John Wiley & Sons; 2006.
- [131] Klimovich PV, Shirts MR, Mobley DL. Guidelines for the analysis of free energy calculations. *J Comput Aided Mol Des.* 2015;29:397–411.
- [132] Naden LN, Pham TT, Shirts MR. Linear basis function approach to efficient alchemical free energy calculations. 1. Removal of uncharged atomic sites. *J Chem Theory Comput.* 2014;10:1128–1149.
- [133] Naden LN, Shirts MR. Linear basis function approach to efficient alchemical free energy calculations. 2. Inserting and deleting particles with Coulombic interactions. *J Chem Theory Comput.* 2015;11:2536–2549.
- [134] Shirts MR, Pande VS. Solvation free energies of amino acid side chain analogs for common molecular mechanics water models. *J Chem Phys.* 2005;122:134508.
- [135] Shirts MR, Pitnera JW, Swope WC, et al. Extremely precise free energy calculations of amino acid side chain analogs: comparison of common molecular mechanics force fields for proteins. *J Chem Phys.* 2003;119:5740–5761.
- [136] Shirts MR, Mobley DL, Chodera JD. Chapter 4 alchemical free energy calculations: ready for prime time? In: Spellmeyer D, Wheeler R, editors. Annual reports in computational chemistry. Elsevier; 2007. p. 41–59.
- [137] Wang F, Landau DP. Efficient, multiple-range random walk algorithm to calculate the density of states. *Phys Rev Lett.* 2001;86:2050–2053.
- [138] Poulain P, Calvo F, Antoine R, et al. Performances of Wang-Landau algorithms for continuous systems. *Phys Rev E.* 2006;73:056704.
- [139] Plimpton S. Fast parallel algorithms for short-range molecular dynamics. *J Comput Phys.* 1995;117:1–19.
- [140] McQuarrie DA, Simon JD. Physical chemistry: a molecular approach. 1st ed. Sausalito (CA): University Science Books; 1997.
- [141] Gmehling J, Kolbe B, Kleiber M, et al. Chemical thermodynamics for process simulation. 1st ed. Weinheim: Wiley-VCH Verlag & GmbH Co. KGaA.; 2012.
- [142] De Reuck K, Craven R. Methanol, international thermodynamic tables of the fluid state, vol. 12. London: IUPAC, Blackwell Scientific Publications; 1993.
- [143] Lemmon EW, Span R. Short fundamental equations of state for 20 industrial fluids. *J Chem Eng Data.* 2006;51:785–850.
- [144] Span R, Wagner W. A new equation of state for carbon dioxide covering the fluid region from the triple-point temperature to 1100 K

- at pressures up to 800 MPa. *J Phys Chem Ref Data*. [1996](#);25:1509–1596.
- [145] Lemmon EW, Huber ML, McLinden MO. NIST reference fluid thermodynamic and transport properties – REFPROP. NIST Stand Ref Database. [2002](#);23:v7.
- [146] Dixit S, Crain J, Poon W, et al. Molecular segregation observed in a concentrated alcohol–water solution. *Nature*. [2002](#);416:829.
- [147] Dixit S, Soper AK, Finney JL, et al. Water structure and solute association in dilute aqueous methanol. *Europhys Lett*. [2002](#);59:377.